

Study on Crack Width and Crack Resistance of Eccentrically Tensioned Steel-Reinforced Concrete Members Prestressed by CFRP Tendons

Yu Deng^a, Jinyang Gui^a, Hexin Zhang^{b,*}, Alberto Taliercio^c, Peng Zhang^a, Simon H F Wong^d, Piti Sukontasukkul^e, Afrasyab Khan^f, Lin Li^g, Yunchao Tang^h, Xingyu Chenⁱ

^a School of Civil Engineering and Architecture, Guangxi University of Science and Technology, Liuzhou, China, 545006

^b School of Engineering and the Built Environment, Edinburgh Napier University, 10 Colinton Road, Edinburgh, Scotland, UK, EH10 5DT

^c Department of Civil and Environmental Engineering, Politecnico di Milano, Milan, Italy

^d Faculty of Science and Technology, Technological Higher Education Institute of Hong Kong, 20A Tsing Yi Road, Tsing Yi Island, New Territories, Hong Kong

^e Construction and Building Materials Research Center, Department of Civil Engineering, King Mongkut's University of Technology North Bangkok, Thailand

^f Institute of Engineering and Technology, Department of Hydraulics and Hydraulic and Pneumatic Systems, South Ural State University, Lenin Prospect 76, Chelyabinsk, 454080, Russian Federation

^g College of Urban and Rural Construction, Zhongkai University of Agriculture and Engineering, Guangzhou, China

^h Department of Civil and Architectural Engineering, Tennessee State University, Nashville, TN, 37209, USA

ⁱ School of Civil Engineering and Architecture, Guangxi University, Nanning, China, 545006

Abstract: In recent decades, steel-reinforced concrete (SRC) members under eccentric tension have been adopted more frequently in modern buildings due to the constraints of more complex structural design/detailing that accompanying contemporary architectural creations. Crack resistance of this type of structures has become a critical design consideration but received insufficient research attention in the past. In this context, the anti-cracking performance of prestressed SRC columns reinforced with CFRP tendons under eccentric tensile loads is investigated experimentally and analytically with the following first-hand experimental validations: 1) prestressed CFRP tendons can well strengthen SRC columns under eccentric tensile load and restrain the crack propagation; 2) an increase in the load eccentricity progressively weakened the influence of prestressing tension level on the cracking load; 3) specimens with the higher prestressed tension level, larger longitudinal reinforcement diameter, and flange thickness exhibited greater crack

1 resistance capacity. Furthermore, the plane-section assumption was also validated in this
2 study. A test data-enhanced analytical method was proposed for determining the cracking
3 load of PSRC columns.

4 **Keywords:** steel-reinforced concrete; crack resistance; eccentric tension; bonded
5 prestressed CFRP tendon; prestressed steel-reinforced concrete

6

7 **1. Introduction**

8 SRC structures have offered numerous advantages over reinforced concrete (RC)
9 structures, including reduced section size and improved mechanical properties. SRC has
10 become one of the most popular structures for designing high-rise buildings [1-6]. Its
11 development and popularity can be assigned to its higher bearing capacity and better
12 deformation performance. Moreover, it offers a reduced cross-sectional area and
13 increased structure span. Compared with steel structures, the SRC columns have lower
14 construction costs and greater structural stability. Furthermore, the encased steel shape is
15 tightly wrapped by the external concrete, providing it with fireproofing, tensioning, and
16 buckling resistance [7-9]. Numerous studies have addressed SRC columns, mainly
17 focusing on the mechanical properties in terms of compression, bending, shearing, and
18 torsion, while a limited number of studies have considered its tensile properties [10-12].

19 In recent decades, SRC columns under immense, concrete-unfavourable, tensile
20 loads have become more common in bridge elements, truss transfer layer, and corner
21 columns of low-rise buildings to utilise their prominent mechanical properties, and
22 economical and construction efficiency. Due to the structural complexity of the
23 contemporary architectural innovation, SRC columns may have to undertake adverse
24 eccentric tension when the structural design/detailing for a centrically tensioned
25 member became unworkable. However, lots of large-scale cracks may form in the
26 concrete areas due to its weakness in tension during their normal service life, which needs
27 to be carefully addressed.

1 Itou et al. studied earthquake damage in southern Hyogo, Japan, focusing on the
2 axial and eccentric tension of embedded and non-embedded column feet. The findings
3 showed that the non-embedded column footings which used steel-reinforced concrete
4 were destroyed by bending or shearing in tension [13, 14]. Fu et al. experimentally
5 assessed SRC eccentric columns through static tests and nonlinear finite element analysis,
6 resulting in revised recommendations for the bearing capacity formula [15, 16]. Under
7 medium and rare earthquakes, the stress state of eccentric compression columns, such as
8 side and corner columns of high-rise buildings, was likely to transform due to overturning
9 moments, which converted them from axial or eccentric compression to axial or eccentric
10 tension. Eventually, this phenomenon can easily result in rapid destruction.

11 Furthermore, some adverse effects from the use of SRC structures have been
12 gradually revealed. On the one hand, under the direct tensile load, it is difficult for SRC
13 columns to effectively control and predict the cracking load. Moreover, once the cracks
14 start to develop, cracked concrete quickly exits work and does not involve in the stresses.
15 This results in the rapidly increasing strain at the cracks of the steel bar, leading to
16 large-scale tensile cracks making corrosion and rust unavoidable, thus reducing the
17 structural strength and service life [17]. Prestressing technology, primarily, through the
18 post-tensioning method is one of the popular options to enhance the crack resistance of
19 SRC structures. Prestressing treatment can also prevent corrosion and destruction of the
20 steel upon its exposure to humidity or corrosive environments [18-20]. Scholars have
21 carried out numerous studies on prestressed SRC structures [21, 22].

22 Fibre-reinforced polymer (FRP) composites have been shown to inhibit crack
23 generation and development, structural reinforcement, and material corrosion resistance
24 [23-28]. To promote the application of SRC structures in China, a prestressed steel
25 reinforced concrete (PSRC) structure with CFRP prestressed tendons was proposed by the
26 authors as an alternative to the SRC columns (Fig. 1). The mechanical behaviour of

1 PSRC columns with steel stranded wire has been assessed over the last few years [29,
2 30].

3 Despite the numerous studies in this field, few experimental studies have addressed
4 PSRC columns under eccentric tensile loads, and they were not covered in relevant codes
5 and technical literature. To the best of the authors' knowledge, this study is the first one
6 applying CFRP tendons to PSRC columns under eccentric tensile load. Additionally, the
7 eccentric tensile load was achieved through a loading device with independent
8 intellectual property rights. A total of 11 SRC columns, with a $200 \times 200 \text{ mm}^2$
9 cross-section and height of 1200 mm, were tested under eccentric tensile loads. The test
10 variables were the load eccentricity, prestressing tension level, longitudinal reinforcement
11 diameter, and steel flange thickness. Then, the distribution of initial cracks in the normal
12 service stage, vertical load maximum versus crack width curves, and the cracking load
13 was systematically examined. Moreover, the design, production, and maintenance of
14 these specimens were carried out simultaneously to avoid the influence of other adverse
15 factors, and ensure that specimens with the same parameters and single variables are
16 comparable. A calculation method was proposed for determining the cracking load
17 through the crack distribution of PSRC columns under a combination of tensile and
18 bending loads. Essentially, this study is aimed at:

- 19 a) Study the strength and structural behaviour of the PSRC columns under the
20 eccentric tensile load during the normal operational stage.
- 21 b) Evaluate the contribution of prestressed CFRP tendons to crack suppression in
22 PSRC eccentric tensile columns and the influence of four design parameters on
23 the cracking load and maximum crack width, based on the analysis of the
24 prestressed tension level, load eccentricity, longitudinal reinforcement diameter,
25 and steel flange thickness.

- 1 c) Establish an analytical model for the calculation of cracking load to predict
2 structural cracking.
- 3 d) Analytically assess the effect of prestressed tension level, steel reinforcement
4 diameter, flange thickness, and load eccentricity.
- 5

6 **2. Experimental program**

7 *2.1 Design of specimens*

8 In this study, 11 SRC columns were prepared and tested under eccentric tensile load.
9 Eight PSRC columns were reinforced with prestressed CFRP tendons, while the
10 remaining three SRC columns had no strengthening agent to serve as the contrast
11 specimens. All the specimens had a 200 mm×200 mm cross-section and a height of 1200
12 mm. The design parameters were the prestress tension level of CFRP tendons (λ), the load
13 eccentricity ratio (e/h), the longitudinal reinforcement diameter (d), and the steel flange
14 thickness (t_f). Specifically, prestress tension levels of 40% and 60% were designated,
15 where (λ) is the ratio of the pretension stress applied to the CFRP tendons to its ultimate
16 tensile strength. Load eccentricity ratios (e/h) of 0.1 and 0.4 were considered. Moreover,
17 four longitudinal reinforcements of HRB400 grade steel reinforcements with a diameter
18 (d) of 6 mm or 10 mm were arranged at each corner of the specimens. Meanwhile, two
19 steel flange thicknesses (t_f) of the steel section (6 and 8 mm) were taken into account.
20 Moreover, a 7 mm diameter CFRP tendon was adopted, and the steel section was formed
21 by 150 mm×50 mm×6 mm×6/8 mm steel, of grade Q235 according to the Chinese
22 standards. The total height and width of the steel shape are 50 mm, and the steel flange
23 thickness was 6/8 mm while the web thickness was set at 6 mm. Finally, the stirrups of
24 HPB300 grade steel reinforcements with a diameter of 6 mm (spaced at 100 mm, A6
25 mm@100 mm) were arranged throughout the height of the specimens.

1 To prevent the slipping of steel and concrete, a row of high-strength studs was
2 arranged on the upper and lower flanges of the steel [31]. The loading end was specially
3 designed to ensure precise force transfer. As shown in Fig. 2, the loading endplate and
4 concrete end of the specimen have a transition zone in compliance with the requirements
5 of prestressed anchoring and tensioning. To replicate the real scenario of a member under
6 eccentric tension in a building, i.e. the eccentric tension force is distributed by the
7 “rigid” joint to the member under the plane-remains-plane assumption, the longitudinal
8 reinforcement, section steel and stiffeners were welded to the loading- endplates. The
9 eccentric tension force is applied and distributed through the endplates.

10 Specimens were labelled as APZ, SPZ, and LPZ corresponding to the axial tension
11 specimens with an eccentricity ratio of 0, small eccentric tension specimens with an
12 eccentricity ratio of 0.1, and large eccentric tension specimens with an eccentricity ratio
13 of 0.4, respectively. For prestressed columns, their label contains three numbers
14 representing the longitudinal reinforcement diameter, steel flange thickness, and
15 prestressed tension level. However, the label of the non-prestressed columns only had two
16 numbers, indicating their longitudinal reinforcement diameter and steel flange thickness.
17 The detailed parameters of the specimens are listed in Table 1, while the cross-sectional
18 dimensions and geometric structure are depicted in Fig. 2.

19

20 *2.2 Design of prestressed elements*

21 The prestressing tendons using the post-tensioning method and the prestress loss
22 was calculated according to the Code for Design of Concrete Structures (GB50010-2010)
23 [32], as follows.

$$24 \quad \sigma_{pc} = \frac{N_{pII}}{A_n} \quad (1)$$

1
$$N_{pII} = (\sigma_{con} - \sigma_l)A_p \quad (2)$$

2
$$A_n = A_c + \alpha_E A_s \quad (3)$$

3 Where σ_c is the normal stress in the concrete generated by the prestressing; N_{pII} is
4 the total pretension in prestressing reinforcement after the complete prestress loss; and
5 σ_{con} is the tension control stress (MPa, $\leq 0.75 f_{ptk}$); σ_l represents a prestress loss value
6 (MPa); A_n is the net cross-sectional area; A_p and A_c are the areas of the prestressing
7 CFRP tendon and the concrete (mm^2), respectively; A_s stands for the area of the
8 steel(mm^2); α_E is the converted modulus of elasticity.

9 After 28 days of pouring and curing, the specimens underwent the pretension
10 process, using the post-tensioning method through self-designed equipment, as shown in
11 Fig.3. Fig. 3(a) provides a detailed view of the setup clearly, illustrating the components
12 of the device while Fig. 3(b) shows an image of the setup.

13 The anchor design was employed to decrease the prestress loss and ensure no
14 failure of CFRP tendons at the anchored region [27]. The CFRP anchors, with an
15 anchoring rate of 1.0, were supplied by OVM (Guang Xi CO., LTD). Two sets of
16 hexagonal anchors and metal spacers were included in the post-tensioning equipment.
17 One was placed after the reaction plate, called working anchor #1, and the other was
18 located before the concrete end of the specimens, called post-tensioning anchor #2, for
19 tightening and releasing the force after each tensioning level.

20 The stressing force was generated using the mono strand hydraulic jacks of 3 tons
21 seated on a special tensioning support. Upon operation, the hydraulic jacks indirectly lift
22 the reaction plate to achieve simultaneous tensioning of the extension screw and CFRP
23 tendons. Note that one end of each CFRP tendon was connected to an extension screw via
24 a connecting sleeve, allowing the CFRP tendons to be indirectly tensioned by tensioning

1 the extension screw which transmitted the tension force. Strain gauges were pasted on the
2 surface of the CFRP tendons to measure the tensioning force due to the hydraulic jack.
3 This method offers more accurate stress data as compared with those only using load cells.
4 The stressing procedure involved the following stages. First, the CFRP tendons were
5 stressed with an initial force of approximately 10% of the total stressing force, F_s , to
6 close the gaps between components and to remove the slack. F_s was then computed from
7 the control stress in the tendons, which was taken as $0.75 f_{pu}$ for CFRP tendons. In the
8 second step, CFRP tendons were stressed at six load levels (40% and 60% of total
9 stressing force), as shown in Table 2. Load cells and strain gauges were attached to CFRP
10 tendons to monitor and measure the stresses in the tendons during the whole
11 post-tensioning process.

12

13 *2.3 Material properties*

14 The mechanical properties of the materials are listed in Table 3. CFRP tendons with
15 a diameter of 7 mm were used, which were supplied by OVM (Guang XI CO., LTD)
16 whose mechanical properties were determined by the tensile test. The properties of the
17 ZH-1 grout material were determined by compression tests on six prisms, splitting tensile
18 tests on six cubes, and bending tests on six prisms. The average compressive strength,
19 splitting tensile strength, and flexural strength were 104.1 MPa, 13.9 MPa, and 38.4 MPa,
20 respectively.

21 Pre-mixed concrete of C40 was used in the test which was supplied from a local
22 concrete manufacturer. The properties of the concrete were determined according to the
23 Chinese standards (GB/T50152-2012) [33]. Twelve concrete test cubes and nine concrete
24 test prisms were simultaneously used and cured along with the test specimens. The test
25 cubes were 150 mm in length, width, and height, while the test prisms were 150 mm in

1 length and width, and 300 mm in height. On the day of testing, the average compressive
2 strength (f_{cu}) and tensile strength (f_c) of the concrete cubes were 27.4 MPa and 2.83
3 MPa, respectively. Using conventional steel bars as longitudinal and transverse steel
4 reinforcements, the ultimate tensile strengths of the longitudinally deformed
5 reinforcements, C10, C6, and transverse steel deformed reinforcements, C6, were found
6 to be 699 MPa, 608MPa and 608 MPa, respectively. Shape steel of grade Q235 and
7 loading endplate of grade Q345 were also applied, whose mechanical properties were
8 reported by the manufacturer after testing six coupons steel specimens according to
9 Chinese standards (JGJ138-2016) [34]. Detailed properties of all the materials are
10 presented in Table 3.

11

12 *2.4 Measurements, test set up, and loading*

13 Fig. 4 illustrates the details of the setup of the self-developed tension-compression
14 conversion frame for applying the eccentric tensile load. This frame consists of an
15 external and internal truss; the top plate of the outer truss and the bottom plate of the
16 inner truss were fitted with hinged supports. Each of the specimen loading endplates was
17 flexibly connected to the hinged supports by high-strength bolts and nuts, to simulate the
18 real force state. Upon applying pressure by a hydraulic compression machine with a
19 capacity of 5,000 kN to the inner truss, the conversion frame will convert the pressure
20 into a tensile load. Pre-loading was applied, up to 5% of the predicted ultimate capacity,
21 to eliminate the gap between the devices. To accurately observe cracks, before and after
22 the occurrence of the first crack, the applied load was stopped and hold at 5 kN and 20
23 kN intervals, respectively. A smaller interval before cracking was used to range the
24 cracking load more accurately as it is one of the key parameters in this study. A larger
25 interval was adopted after cracking to minimise the impact of the temporary holds to the
26 overall loading and to reduce the total testing time. And all the specimens were

1 progressively tested under monotonic loads up to yield.

2 The layout of the linear variable displacement transducers (LVDTs) and strain
3 gauges are presented in Fig. 5. During the loading process, five LVDTs (D₁-D₅) were
4 arranged along the height of the specimen to measure the lateral deflections. To monitor
5 the response of the strain, four (T₁-T₄), nine (T₅-T₁₃), and five (T₁₄-T₁₈) strain gauges
6 were attached to the longitudinal reinforcement, steel shape, and concrete surface at the
7 mid-height of the specimen, respectively. Additionally, four strain gauges (C₁-C₄) were
8 bonded on the CFRP tendons to measure strain responses and stress loss of the CFRP
9 tendons, as depicted in Fig. 5.

10 It is worth mentioning that vertical load was applied to the specimen by the loading
11 endplate welded to the steel shape and the longitudinal reinforcement. Various
12 eccentricities were achieved by changing the position of hinge support at the loading end
13 of the specimen, as shown in Fig. 4.

14

15 **3. Test results and analysis**

16 *3.1 Test phenomenon*

17 The results of all the specimens are shown in Table 4, where P_u is the peak load.

18 Initial cracks: For specimens with eccentricity ratios of 0, 0.1, and 0.4, the
19 horizontal tensile cracks occurred in the tension side of the specimens, when the load
20 reached approximately $0.22 P_u$, $0.25 P_u$ - $0.34 P_u$, and $0.18 P_u$ - $0.24 P_u$ respectively. Most of
21 the horizontal tensile cracks occurred within the middle 1/3 of the specimen height,
22 started from the tension side and propagated towards the compression side across the
23 cross-section. The reason that the tensile cracks started at the middle section is due to the
24 combined effect of tension and bending which formed a maximum tension zone at the

1 middle section of the column. The number of initial cracks of all specimens ranged in 1-3
2 which propagated slowly with increasing the load.

3 The overall distribution of cracks: Although the horizontal cracks of all the
4 columns developed at a uniform speed with load increment, no diagonal cracks were
5 observed in the middle of the specimen. Compared with non-prestressed columns, the
6 initial cracks of prestressed columns appeared later with significantly lower quantity. The
7 vertical cracks at the endplate developed rapidly at the yield load, where the crack height
8 ranged from 150 mm to 320 mm.

9 *3.2 Crack analysis*

10 The fundamental objective of this article is to enhance the crack resistance of SRC
11 columns during normal service life through the use of prestressing tendons. As a result,
12 the cracking load and maximum crack width are the central concerns, however, failure
13 modes of the specimens are not discussed here. The crack distribution (right elevation) of
14 all the columns during normal use is shown in Fig. 6. Combined with the test
15 phenomenon, the studies on crack propagation regularity can be obtained as follows:

16 There is no significant difference in the patterns of tension crack distribution for all
17 the columns with eccentricity ranges from 0.1 to 0.4. The diagonal cracks close to the end
18 of the column, however, show distinguishing differences among them. For five test
19 specimens with an eccentricity of 0.1, the initial cracks appeared on the eccentric and
20 non-eccentric load sides of the specimen. By continuing the load application, most cracks
21 gradually penetrated the entire section of the specimen. This phenomenon is similar to
22 that of the axial tension specimen with no eccentricity. This is because for small eccentric
23 specimens, the distance of eccentricity is much smaller than the section height, so the
24 performance of small eccentric specimens is very little different from the non-eccentric
25 ones. Another more important reason is that the CFRP prestressed tendon counteracts the
26 eccentric load and offset the effect of small eccentricity so that there is no significant

1 difference to the axial tension. Also, the concrete was directly subjected to tensile stress,
2 resulting in random cracks that could easily penetrate throughout the cross-section.

3 For five large eccentric columns with an eccentricity of 0.4, horizontal cracks
4 developed from the applied eccentric load side to the other side. Most of the cracks did
5 not propagate through the entire section and crack height was close to the cross-section
6 height of the specimen. Owing to the large eccentricity, the neutral axis of the
7 cross-section appeared as the load progressed, and the concrete near the applied eccentric
8 load side was subjected to tension, while the other side experienced compression. Cracks
9 are likely to appear in the tension zone due to the lower tensile strength of concrete.

10 Based on Fig. 6, as the prestress tension level increased from 0% to 40% and then
11 to 60%, the number of cracks and reduced. A significant decline can be observed in the
12 number of cracks upon raising the prestress tension level from 40% to 60%. As the
13 diameter of the longitudinal reinforcements ranged from 6 mm to 10 mm, The number
14 and spacing of cracks remain essentially unchanged, but there is some reduction in crack
15 width for columns with an eccentricity of 0.4. The longitudinal reinforcement diameter
16 showed a more obvious effect on the specimens with a larger eccentricity. However, the
17 flange thickness limitedly influenced crack distribution, number, and spacing on eccentric
18 columns with an eccentricity of 0.4.

19 20 *3.3 Maximum crack width analysis*

21 Under short-term service load, the maximum crack widths of concrete were
22 carefully measured by the ZW-F160 crack width tester. The relationships between design
23 parameters and the maximum crack width of the midspan zone in the normal limit
24 condition are shown in Fig.7. After comparison, the following conclusions can be drawn.

25 As shown in Fig. 8(a), with increasing the eccentricity, the maximum crack widths
26 of the specimen with the eccentricity ratio of 0.1 are significantly smaller than the one

1 having the eccentricity ratio of 0.4, indicating the detrimental role of the eccentricity
2 growth in crack control of SRC tensile columns. This phenomenon can be explained by
3 the fact that the tensile load is close to the concrete edge on the eccentric side when the
4 eccentricity ratio reached 0.4, which will greatly weaken the restraint of the stirrups on
5 the concrete.

6 However, the crack width of SPZ-6-6 is smaller than APZ-6-6, which is related to
7 the heterogeneity and anisotropy of the concrete but is also a good indication of the
8 eccentric specimens with an eccentricity ratio of 0.1 and the axial tension member have
9 similar mechanical properties in terms of the resistance to crack width propagation.

10 Fig. 7(b) also highlights that maximum crack width can be effectively decreased by
11 prestress level. The level of prestressing is inversely proportional to the rate of crack
12 propagation. This can be attributed to two aspects: 1) the prestressing technique can
13 effectively provide the specimens with pre-compression stress to offset the
14 load-generated tensile stress before the cracks arise; 2) CFRP tendons can increase the
15 bending stiffness to delay the crack propagation after its occurrence. Fig. 7(c-d) reveal
16 that the increase in longitudinal reinforcement and flange thickness of the steel section
17 could have a mixed effect on the crack resistance. The level of the eccentricity, the
18 ultimate tensile force achieved in the tests all have an impact on the maximum crack
19 width.

20

21 *3.4 Cracking load analysis*

22 Table 4 lists the cracking load values of eleven specimens. The following
23 conclusions can be obtained.

24 The eccentricity ratios of non-prestressed columns (APZ-6-6, SPZ-6-6, and
25 LPZ-6-6) with the same flange thickness and longitudinal reinforcement diameter were 0,
26 0.1, and 0.4, respectively. By incrementing the eccentricity ratio from 0 to 0.1 and then to

1 0.4, the cracking load was reduced by 9.3% and 46.6%, respectively, reflecting the
2 significant influence of loading eccentricity on the cracking load of the tensile columns.

3 The eccentricity ratios of prestressed columns (SPZ-6-6-40, LPZ-6-6-40,
4 SPZ-6-6-60, and LPZ-6-6-60) with the same flange thickness and longitudinal
5 reinforcement diameter were 0.1, 0.4, 0.1, 0.4, respectively. Raising the eccentricity ratio
6 from 0.1 to 0.4 decremented the cracking load by 47.6%, in SPZ-6-6-40 and LPZ-6-6-40,
7 and 42.7% in SPZ-6-6-60 and LPZ-6-6-60. Therefore, regardless of prestressing, the
8 eccentricity ratio is an important parameter of cracking load.

9 For similar loading eccentricity, flange thickness, and longitudinal reinforcement
10 diameter, the prestressed tensile levels of the small eccentric columns (SPZ-6-6,
11 SPZ-6-6-40, and SPZ-6-6-60) were 0%, 40%, and 60%, respectively. An increment in the
12 prestressed tension level from 0% to 40% and then to 60% enhanced the cracking load by
13 64.8% and 22.8%, respectively. Similarly, for large eccentric columns (LPZ-6-6,
14 LPZ-6-6-40, and LPZ-6-6-60) with the same eccentricity, flange thickness, and
15 longitudinal reinforcement diameter, the prestressed tensile levels were 0%, 40%, and
16 60%, respectively. A rise in the prestressed tensile level from 0% to 40% and then to 60%
17 elevated the cracking load by 61.7% and 34.2%, respectively. These findings indicate the
18 decisive role of the prestressed tension level in boosting the cracking load of the
19 specimen.

20 For prestressed small (SPZ-6-6-40 and SPZ-10-6-40) and large, (LPZ-6-6-40 and
21 LPZ-10-6-40) eccentric columns, the only difference was the longitudinal reinforcement
22 diameter. By increasing the longitudinal reinforcement diameter from 6 to 10 mm, the
23 cracking load was enhanced by 6.6% and 6.9%, respectively. Therefore, the longitudinal
24 reinforcement diameter is also an important factor in the cracking load.

25 For the prestressed columns of LPZ-6-6-40 and LPZ-6-8-40 and SPZ-6-6-40 and
26 SPZ-6-8-40, the flange thickness is the variable parameter. Upon increasing the flange

1 thickness from 6 to 8 mm, the cracking load was also increased by 3.0% and 0.3%,
2 respectively, suggesting the influence of flange thickness on the cracking load. Its impact
3 is, however, limited compared with the other design parameters.

4 Comparing prestressed eccentric columns and non-prestressed axial tensile columns
5 (APZ-6-6), the cracking load of prestressed small eccentric columns (SPZ-6-6-40,
6 SPZ-6-6-60, SPZ-10-6-40, and SPZ-6-8-40) showed 49.5%, 83.5%, 59.8%, and 49.5%,
7 enhancement, respectively; the rate of change in prestressed large eccentric columns
8 (LPZ-6-6-40, LPZ-6-6-60, LPZ-10-6-40, and LPZ-6-8-40) was -21.6%, 5.2%, -16.5%
9 and -18.6%, respectively. Except for LPZ-6-6-60, the crack resistance was less than that
10 of the non-prestressed axial tension member (APZ-6-6). At a lower prestress level, the
11 load eccentricity showed a limited impact on the cracking load, while the cracking load
12 improved faster as the prestress level increased. The main cause of this phenomenon is
13 the crack resistance and strengthening effect of the CFRP tendons, which outperformed
14 the weakening effect of the eccentricity.

15 In general, the cracking load increases as the eccentricity decreases and the
16 increment in the prestressed tension level, longitudinal reinforcement diameter, and
17 flange thickness. Among these four design parameters, the prestressed tension level and
18 eccentricity showed the most significant influence on the cracking load. The effect of the
19 longitudinal reinforcement diameter was slightly smaller, whereas the flange thickness
20 did not remarkably affect the cracking load. The crack resistance of prestressed small
21 eccentric columns was much higher than that of non-prestressed axial tension columns.
22 Moreover, when the CFRP tendons reached a higher prestressed tension level, the crack
23 resistance of prestressed large eccentric columns also improved to a certain extent
24 compared to non-prestressed axial tension columns. The above discussion shows the
25 remarkable tension properties of CFRP tendons which could improve the capacity to
26 delay the emergence of cracks in eccentric specimens. Furthermore, the crack resistance

1 of some prestressed large eccentric columns was even better than that of non-prestressed
2 axial tensile columns, suggesting the crack-postponing role of prestressing.

3

4 **4. Cracking load and maximum crack width calculation**

5 It was assumed that the stress curves of the tensile and compressive concrete are
6 triangular just before cracking [35].

7 *4.1 Elastic analysis and calculation of the pressure relief stage*

8 For SRC specimens, the axial and bending deformation occurred during the test.
9 Numerous studies have developed calculation methods for determining sectional capacity
10 [36]. However, the cracking load should be emphatically focused; as the crack resistance
11 is a vital index in evaluating structural performance. Furthermore, crack control is the
12 essential factor to ensure the normal function and durability of the structure. In this paper,
13 the strength of the steel shape and longitudinal reinforcement of all the specimens was far
14 from the yield strength before the initial cracks arise. Therefore, the elastic stress theory
15 can be used to calculate the cracking load of PSRC columns. The following assumptions
16 were considered:

17 (1) The CFRP tendons, steel shape, and concrete are ideal elastomers. The stress
18 and strain of the CFRP, steel shape and longitudinal reinforcements show a linear
19 relationship, without considering the strengthening period.

20 (2) In this study, the specimens were designed to have a full shear connection to
21 prevent the premature failure of the shear connectors. Moreover, the CFRP anchorage
22 works well without failure or slip.

23 (3) The plane-section assumption is satisfied.

24

1 4.1.1 Elastic analysis

2 Considering the above assumptions, the anti-cracking capacity of PSRC columns
 3 under eccentric tensile load can be determined according to the elastic modulus ratio of
 4 the steel shape, CFRP tendons, and longitudinal reinforcements. All the materials were
 5 converted to concrete to simplify the calculation process; the detailed steps are shown in
 6 Fig. 8.

$$7 \quad n_p = \frac{E_p}{E_c}; \quad n_a = \frac{E_a}{E_c}; \quad n_s = \frac{E_s}{E_c} \quad (4)$$

8 Where n_p, n_a, n_s are the conversion modulus of the elastic modulus of CFRP tendons,
 9 section steel, and longitudinal reinforcement, respectively; E_p, E_c, E_s and E_a denote the
 10 elastic modulus of CFRP, concrete, longitudinal reinforcement, and section steel,
 11 respectively.

$$12 \quad A_n = bh + (n_a - 1)A_a + (n_s - 1)(A'_s + A_s) - A_k \quad (5)$$

13 Where A_n is the net cross-sectional area of converted concrete; A_p, A'_s, A_s, A_a, A_k
 14 represent the cross-sectional areas of the CFRP tendons, upper and lower longitudinal
 15 reinforcements, steel shape, and prestressed tendon apertures, respectively.

$$16 \quad y_{In} = \frac{(n_s - 1)[A'_s a'_s + A_s (h - a_s)] - A_k (h - a_p)}{A_n} + \frac{bh^2 / 2 + (n_a - 1)hA_a / 2}{A_n} \quad (6)$$

17 As shown in Fig. 9, where y_{In} shows the distance from the cross-sectional centroid
 18 to the concrete edge of the CFRP tendons side; a_s and a_p are the distances from the
 19 centroid of longitudinal reinforcement and CFRP tendons to the bottom of the
 20 cross-section.

$$21 \quad y_{2n} = y - y_{In} \quad (7)$$

1 Where y_{2n} is the distance from the centroid of the section to the edge of the concrete
2 away from the side of the prestressed CFRP reinforcement.

$$3 \quad I_n = (n_s - 1)[A'_s(y_{1n} - a'_s)^2 + A_s(h - y_{1n} - a_s)^2] + (n_a - 1)[I_a + A_a(y_{2n} - h/2)^2] + bh^3/12 +$$

$$4 \quad bh(y_{1n} - h/2)^2 - A_k(y_{2n} - h + a_p)^2$$

$$5 \quad (8)$$

6 In which I_n and I_a are the inertia moments of the net section of concrete and
7 section steel, respectively.

8

9 *4.1.2 Calculation of the decompression stage*

10 In this test, grouting of all the prestressed specimens began when the tensioning
11 work was completed, and the loading test was carried out immediately after fifteen days
12 of prestressing monitoring. It can be assumed that the prestress losses were finished.
13 Based on the actual conditions of the test, the resultant force, N_{pe} , at the joint point can
14 be obtained by:

$$15 \quad N_{pe} = \sigma_{pe}A_p - \sigma_{l5}(A_s + A'_s + A_a) \quad (9)$$

16 Where σ_{pe} is the effective prestress, σ_{l5} is the prestress loss value caused by
17 prestress relaxation, shrinkage, and creep of concrete, and A_p denotes the area of CFRP
18 tendons.

19 In the full-section decompression stage, the pre-stress produces normal stress on
20 the specimen section, thus the normal stress of concrete, σ'_{pc} , can be expressed as:

$$21 \quad \sigma'_{pc} = -\frac{N_{pe}}{A_n} \pm \frac{N_{pe} \times e_{pn}}{I_n} y_{1n} \quad (10)$$

1 Where e_{pn} shows the distance from the centroid of the net section to the applied
2 load point.

3 For zero normal stress of concrete at the joint point, the CFRP tendon stress, σ_{p0} ,
4 can be expressed as:

$$5 \quad \sigma_{p0} = (\sigma_{con} - \sigma_l) + \alpha_p \sigma_{pc} \quad (11)$$

6 After decompression, the joint forces, N_{p0} , will be:

$$7 \quad N_{p0} = \sigma_{p0} \times A_p \quad (12)$$

8

9 4.2 Cracking load calculation

10 With reference to the Code for Design of Composite Structures JGJ138-2016, the
11 theory for calculating the bearing capacity of eccentric tensile columns and the theory of
12 cracking resistance for ordinary columns, the following basic assumptions were made:

13 (1) When the eccentric load is applied to the exterior of the section, there will be a
14 compressive zone in the cross-section; while the eccentric load is applied to the interior of
15 the section, the whole cross-section of the member will be in tension.

16 (2) The eccentricity ratio affects the concrete stresses at the edge of the section,
17 which is linearly proportional to the ratio.

18 (3) The stiffness of different parts in a cross-section will affect the distribution of the
19 stresses following the stress-strain relationship.

20 Under short-term tensile load, eccentricity is one of the most important factors that
21 determine the crack resistance for PSRC columns. And a load eccentricity ratio
22 coefficient φ is proposed to estimate the adverse effect of eccentricity on cracking.

23

$$24 \quad \varphi = \frac{h-2e}{h} = 1 - 2\left(\frac{e}{h}\right) \quad (13)$$

25

1 While the prestressed CFRP tendons are only arranged on the tension zone
 2 eccentrically, it can assume that the section stiffness between the two sides of the member
 3 axis is different. For the stress-strain relation in the cracked section, the central axis is
 4 used as the separation line, and only the eccentricity ratio is considered in the lower part,
 5 while the stiffness and the eccentricity are considered in the upper part. The stiffness
 6 coefficient k is proposed, and combined with the experimental data, the weakening effect
 7 of stiffness is significantly smaller than the eccentricity ratio. In order to ensure safety
 8 and simplification of calculation, k can be taken as:

$$9 \quad k = \varphi \quad (14)$$

10 When tensile loads are applied within the section of the member ($0 \leq \varphi \leq 1$), this
 11 means that the full section of the member is subjected to tension, as shown in Fig.9.

12 According to Fig.9, the strain of all materials can be obtained at once.

$$13 \quad \varepsilon_c = 0.5\left(\frac{1+\varphi}{2} + 1\right)\varepsilon_{cr} \quad (15)$$

$$14 \quad \varepsilon'_c = 0.5\left(\frac{1+\varphi}{2} + \varphi\right)\kappa\varepsilon_{cr} \quad (16)$$

$$15 \quad \varepsilon_p = \left[\varphi + \frac{h-a_p}{h}(1-\varphi)\right]\varepsilon_{cr} \quad (17)$$

$$16 \quad \varepsilon_{af} = \left[\varphi + \frac{h-a_{af}}{h}(1-\varphi)\right]\varepsilon_{cr} \quad (18)$$

$$17 \quad \varepsilon'_{af} = \left[\varphi + \frac{a'_{af}(1-\varphi)}{h}\right]\kappa\varepsilon_{cr} \quad (19)$$

$$18 \quad \varepsilon_s = \left[\varphi + \frac{h-a_s}{h}(1-\varphi)\right]\varepsilon_{cr} \quad (20)$$

$$19 \quad \varepsilon'_s = \left[\varphi + \frac{a'_s(1-\varphi)}{h}\right]\kappa\varepsilon_{cr} \quad (21)$$

20
 21 The cracking load N_{cr} of the PSRC member can be expressed as follows from the
 22 principle superposition:

$$23 \quad N_{cr} = \frac{E_c}{2}(A_c\varepsilon_c + A'_c\varepsilon'_c) + A_p E_p \varepsilon_p + b_f t_f E_a (\varepsilon_{af} + \varepsilon'_{af}) + \frac{h_f - 2t_f}{2} t_w E_a (\varepsilon_{aw} + \varepsilon'_{aw}) + A_s E_s \varepsilon_s + A'_s E_s \varepsilon'_s \quad (22)$$

1

2 In addition, when tensile loads are applied to the outside of the section($\varphi < 0$), it is
3 clear that the tension zone and the compression zone are existing at the same time.

$$4 \quad N_{cr} = \frac{f_t + \varphi f_c}{2} A_c + b_f t_f E_a (\varepsilon_{af} + \varphi \varepsilon'_{af}) + A_s E_s \varepsilon_s + \frac{1 + \varphi}{2} (h_f - 2t_f) t_w E_a \varepsilon_{aw} + \varphi A'_s E_s \varepsilon'_s \quad (23)$$

5 The experimental value and calculated value of cracking load are listed in Fig.10,
6 numbers 1 to 11 represent APZ-6-6 ~ LPZ-6-8-40 in that order. As indicated, the
7 predicted values are generally in good agreement with the experimental results. The
8 average value of the ratio between calculation and test results is 0.97 and their
9 corresponding standard deviations is 0.11. The test value is slightly smaller than the
10 calculated value which can be assigned to three main reasons. Firstly, the columns with
11 tensile and bending loads are more susceptible to concrete heterogeneity. Secondly, the
12 connection joints between the member and the hinge support have a lateral displacement
13 space of 5 mm due to the installation error, which may result in torsional interference
14 during the loading process. Thirdly, the upper and lower steel flanges of the member are
15 provided with high-strength studs, which are subjected to large shear forces under tensile
16 loading. Therefore, this would accelerate the formation of internal micro-cracks around
17 the stud.

18 However, calculation error (μ_1) of cracking load of all the specimens varied from 1%
19 to 17% in Table 5, with an average ratio of 0.97 and a coefficient of variation of 0.11,
20 reflecting the accuracy of the calculation formula. As a result, the established formulas
21 are validated and can be used to evaluate the cracking capacities of PSRC columns in
22 practice.

23

24 *4.3 The crack width calculation*

Code for Design of Concrete Structures (GB50010-2010) [32] and Code for Design of Composite Structures (JGJ 138-2016) [34] provide the method for evaluating the maximum crack width of concrete (ω_{\max}) based on the theory of bonding-slip.

$$\omega_{\max} = \alpha_{cr} \psi \frac{\sigma_{sq}}{E_s} \left(1.9c_s + 0.08 \frac{d_{eq}}{\rho_{te}} \right) \quad (24)$$

with

$$\psi = 1.1 - 0.65 \frac{f_{tk}}{\rho_{te} \sigma_{sq}} \quad (25)$$

and

$$d_{eq} = \frac{\sum n_i d_i^2}{\sum n_i v_i d_i} = \frac{4(A_s + A_p + \zeta A_a)}{\sum n_i v_i d_i} \quad (26)$$

$$\rho_{te} = \frac{A_s + A_p E_p / E_s + \zeta A_a E_a / E_s}{A_n} \quad (27)$$

where α_{cr} is force characteristic coefficient; ψ is the unevenness coefficient of tensile stress of longitudinal reinforcement; σ_{sq} is the equivalent stress of longitudinal reinforcement; c_s is the distance from the outer edge of the outside tension longitudinal reinforcement to the bottom edge of tension zone; d_{eq} is the effective diameter of tensile materials; ρ_{te} is the equivalent ratio of longitudinal tensile reinforcement calculated by effective tensile concrete cross-sectional area; f_{tk} is standard values for axial tensile strength of concrete; c_f is crack calculation coefficient, axial tension columns $c_f=1.1$, eccentric tension columns $c_f=1.0$; d_i, n_i, v_i are the i -th longitudinal reinforcement diameter, number and relative bond characteristics in the tensile zone, respectively.

1 As a proportional coefficient of steel tensile area, the parameter ζ is introduced in
2 this paper to predict the ratio of tensile area steel to the total area of steel, small eccentric
3 tensile columns ($e/h=0.1$) with $\zeta=1$ and large eccentric tensile columns ($e/h=0.4$) are
4 calculated as follows.

$$5 \quad \zeta = [1 - (x - a'_{af}) / (h - a'_{af} - a_{af})] \quad (28)$$

6 where x is the height of the compression zone of the member section

7 A comparison of calculation and experimental results of maximum crack widths is
8 presented in Fig. 11. It could be found that the calculation results for the modified method
9 relatively agree well with the experimental results. The Experimental and analytical values for
10 the maximum crack width of the specimens are summarized in Table 6. The average value of the
11 ratio between calculation and test results is 0.96 and their corresponding standard
12 deviations is 0.29.

14 **5. Conclusion**

15 An experimental study was conducted to investigate the crack resistance of
16 eccentrically tensioned SRC Members that are prestressed by CFRP Tendons. Eight
17 prestressed specimens and three non-prestressed specimens were fabricated and tested.
18 An test data-enhanced analytical model and a set of design formulas for estimating the
19 crack load and crack resistance were proposed. The main findings can be summarized as
20 follows:

- 21 1. Carbon fibre reinforced polymer (CFRP) tendons were successfully used as
22 prestressed tendons for SRC members under eccentric tension. Their performance
23 meets the structural requirements.

- 1 2. The crack resistance has a negative correlation with eccentricity but a positive
2 correlation with prestressing tension level, longitudinal reinforcements diameter,
3 and steel flange thickness.
- 4 3. The cracking load of the PSRC member was enhanced by the prestress effect. The
5 prestressed members exhibited higher crack resistance that has led to improved
6 structural safety, durability and service life.
- 7 4. The analytical model proposed considered three possible positions of the neutral
8 axis and was used to estimate the cracking load and crack width. This analytical
9 calculation shows good agreement with the experimental result.

11 **Acknowledgements**

12 The authors would like to express their special gratitude to the supports from the
13 National Nature Science Foundation of China (51768008), British Council and Ministry
14 of Education, China (UK-China-BRI Countries Education Partnership Initiative), China
15 Postdoctoral Science Foundation Project (2017M613273XB), and Nature Science
16 Foundation of Guangxi Zhuang Autonomous Region (2019JJA160137) and Liuzhou
17 Scientific Research and Technology Development Plan (2017BC40202), Royal Academy
18 of Engineering-Visiting Professor (VP2021\7\12), and Royal Academy of
19 Engineering-Industrial Fellowship (IF\192023).

1
2
3
4
5
6
7
8
9
10
11
12
13
14
15
16

17 **References**

- 18 1. Oehlers, D., D.J. Oehlers, and M.A. Bradford, *Elementary behaviour of composite steel and*
19 *concrete structural members*. 1999: Elsevier.
- 20 2. Jeong, Y., S.H. Kim, and J.H. Ahn, *Partial-interactive behaviour of steel–concrete members under*
21 *static and fatigue loadings*. Magazine of Concrete Research, 2005. **57**(5): p. 289-300.
- 22 3. Zhang, J. and J. Jia, *Experimental study on seismic behavior of composite frame consisting of SRC*
23 *beams and SRUHSC columns subjected to cyclic loading*. Construction and Building Materials,
24 2016. **125**: p. 1055-1065.
- 25 4. Melbourne, C., *Composite structures of steel and concrete, Volume 1: Beams, slabs, columns, and*
26 *frames for buildings*. Engineering Structures, 1997. **4**(19): p. 338.
- 27 5. Ebadi Jamkhaneh, M., M.A. Kafi, and A. Kheyroddin, *Behavior of partially encased composite*
28 *members under various load conditions: Experimental and analytical models*. Advances in
29 Structural Engineering, 2019. **22**(1): p. 94-111.
- 30 6. Hansapinyo, C., et al., *Residual Strength of Reinforced Concrete Beams under Sequential Small*
31 *Impact Loads*. Buildings, 2021. **11**(11): p. 518.
- 32 7. Linhai Han, K.Z., Qinghua Tan, et al. , *Performance of steel reinforced concrete columns after*
33 *exposure to fire: Numerical analysis and application*. . Engineering Structures, 2020. **211**: p.

- 1 110421.
- 2 8. Qingfeng Xu, C.H., Yong C. Wang, et al. , *Experimental and numerical investigations of fire*
3 *resistance of continuous high strength steel reinforced concrete T-beams*. . Fire Safety Journal,
4 2015. **78**: p. 142-154.
- 5 9. Zihua Zhang, J.L., Lei Zhang, et al. , *Study on the interfacial shear behavior of steel reinforced*
6 *concrete (SRC) members with stud connectors after fire*. Frontiers of Structural and Civil
7 Engineering, 2014. **8**(2): p. 140-150.
- 8 10. Linhai Han, Q.T., Tianyi Song. , *Fire Performance of Steel Reinforced Concrete (SRC) Structures*. .
9 Procedia Engineering, 2013. **62**: p. 46-55
- 10 11. Shiang Zhang, Z.Z., Xiaogang He. , *Flexural behavior of SRC columns under axial and bilateral*
11 *loading*. Applied Mechanics and Materials, 2012. **166-169**: p. 3383-3390.
- 12 12. E.L. Tan, B.U., *Experimental study on curved composite beams subjected to combined flexure and*
13 *torsion*. Journal of Constructional Steel Research, 2009. **65**(8): p. 1855-1863.
- 14 13. ITOU Michio, O.S., TANAKA Hidenori, et al. , *Ultimate strength and ductility of bare type column*
15 *base connection in SRC structures under high axial tension: (part 5) [C] // Summaries of Technical*
16 *Papers of Annual Meeting Architectural Institute of Japan, 2000*. . Tokyo: Architectural Institute of
17 Japan, 2000: , 2000: p. 1141-1142
- 18 14. FUJIWARA Daiei, S.K., ITOU Michio, et al. , *Ultimate strength and ductility of bare type column*
19 *baseconnection in SRC structures under high axial tension: (part 14) [C] // Summaries of Technical*
20 *Papers of Annual Meeting Architectural Institute of Japan, 2004*. Tokyo: Architectural Institute of
21 Japan, 2004: , 2004: p. 1219-1220
- 22 15. Jianping Fu, Q.C., Chuan Zhang., *Calculation for ultimate flexural capacity of eccentrically*
23 *tensioned SRC members with embeded I-shaped steel*. . Journal of Building Structures, 2017. **38**(2):
24 p. 90-98
- 25 16. Jinshu Tang, W.H., Su Zhang, et al. , *Experimental study of mechanical behaviors of SRC beams*
26 *under eccentric tension*. . Industrial Construction, 2015. **45**(8): p. 170-174
- 27 17. Peng Zhang, M.S., Yu Deng. , *Study on eccentric tension test and bearing capacity of SRC members*.
28 Journal of Shenyang Jianzhu University, 2019. **35**(3): p. 453-461
- 29 18. Deng, Y., et al., *Experimental and analytical investigation on flexural behaviour of RC beams*
30 *strengthened with NSM CFRP prestressed concrete prisms*. Composite Structures, 2021. **257**: p.
31 113385.
- 32 19. Deng, Y., et al., *Experimental study on shear performance of RC beams strengthened with NSM*
33 *CFRP prestressed concrete prisms*. Engineering Structures, 2021. **235**: p. 112004.
- 34 20. Deng, Y., et al., *Experimental and Analytical Studies on Steel-Reinforced Concrete Composite*
35 *Members with Bonded Prestressed CFRP tendon under Eccentric Tension* Composite Structures,
36 2021. **Accepted**.
- 37 21. Gangfeng Yao, X.X., *Analytical model and evaluation of maximum crack width for unbonded PSRC*
38 *frame beam under short-term service load*. . The Structural Design of Tall and Special Buildings,
39 2019. **28**(16): p. 1667.
- 40 22. Vu, N.A., A. Castel , and R. Francois *Effect of stress corrosion cracking on stress-strain response of*
41 *steel wires used in prestressed concrete beams*. Corrosion Science, 2009. **51**(6): p. 1453-1459.

- 1 23. M. Baena, A.T., Ll. Torres, et al. , *Experimental study and code predictions of fibre reinforced*
2 *polymer reinforced concrete (FRP RC) tensile members*. *Composite Structures*, 2011. **93**(10): p.
3 2511-2520.
- 4 24. P. Selvachandran, S.A., K. L. Muthuramu. , *Modified frosch crack width model for concrete beams*
5 *prestressed with CFRP bars*. . *Polymers and Polymer Composites*, 2016. **24**(7): p. 587-596.
- 6 25. P. Selvachandran, S.A., K. L. Muthuramu., *Deflection of steel reinforced concrete beam prestressed*
7 *with CFRP bar*. *Archives of Metallurgy & Materials*., 2017. **62**(3): p. 1915-1922.
- 8 26. Tan D. Le, T.M.P., Hong Hao, et al. , *Performance of precast segmental concrete beams*
9 *posttensioned with carbon fiber-reinforced polymer (CFRP) tendons*. . *Composite Structures*, 2018.
10 **208**: p. 56-69.
- 11 27. Ashraf Salah-Eldin, H.M.M., Brahim Benmokran, *Structural performance of high-strength-concrete*
12 *columns reinforced with GFRP bars and ties subjected to eccentric loads*. *Engineering Structures*,
13 2019. **185**: p. 286-300.
- 14 28. Tang, Y., et al., *Axial compression behavior of recycled-aggregate-concrete-filled GFRP–steel*
15 *composite tube columns*. *Engineering Structures*, 2020. **216**: p. 110676.
- 16 29. Yu Deng, X.W., Peng Zhang, *Experimental study on eccentric tensile properties of prestressed steel*
17 *reinforced concrete columns*. *Journal of Building Structures*, 2019. **40**(5): p. 115-123.
- 18 30. Yu Deng, X.W., Peng Zhang, *Experimental study and calculation for crack control of unbonded*
19 *prestressed steel reinforced concrete members under eccentric tension*. . *Industrial construction*,
20 2019. **49**(8): p. 185-189
- 21 31. Yong Yang, Y.C., Wensong Zhang, et al. , *Behavior of partially precast steel reinforced concrete*
22 *columns under eccentric loading*. *Engineering Structures*, 2019. **197**: p. 109429.
- 23 32. *GB50010-2012: Code for Design of Concrete Structures*. 2012, China Academy of Building
24 Research.
- 25 33. *GB/T 50152-2012: Standard for test method of concrete structures*. 2012, China Academy of
26 Building Research.
- 27 34. *JGJ 138-2016: Code for design of composite structures*. 2016, China Academy of Building
28 Research.
- 29 35. Qi Cao, J.Z., Zhimin Wu, et al. , *Flexural behavior of prestressed CFRP reinforced concrete beams*
30 *by two different tensioning methods*. . *Engineering Structures*, 2019. **189**: p. 411-422.
- 31 36. Tan D. Le, T.M.P., Hong Hao, et al. , *Flexural behaviour of precast segmental concrete beams*
32 *internally prestressed with unbonded CFRP tendons under four-point loading*. *Engineering*
33 *Structures*, 2018. **168**: p. 371-383.

34

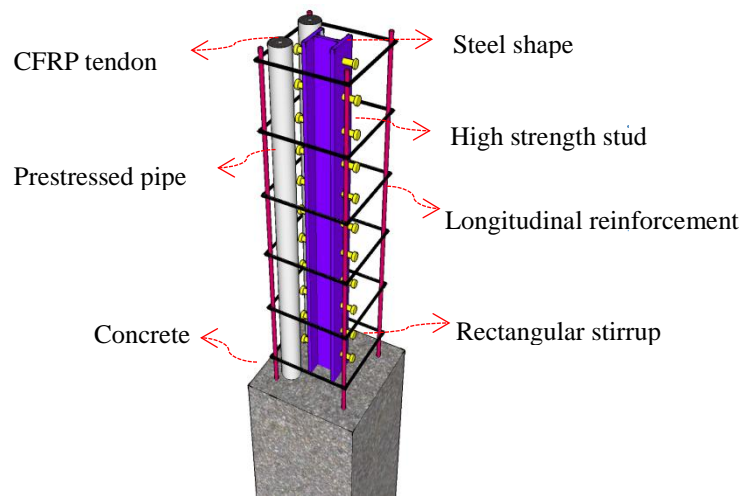
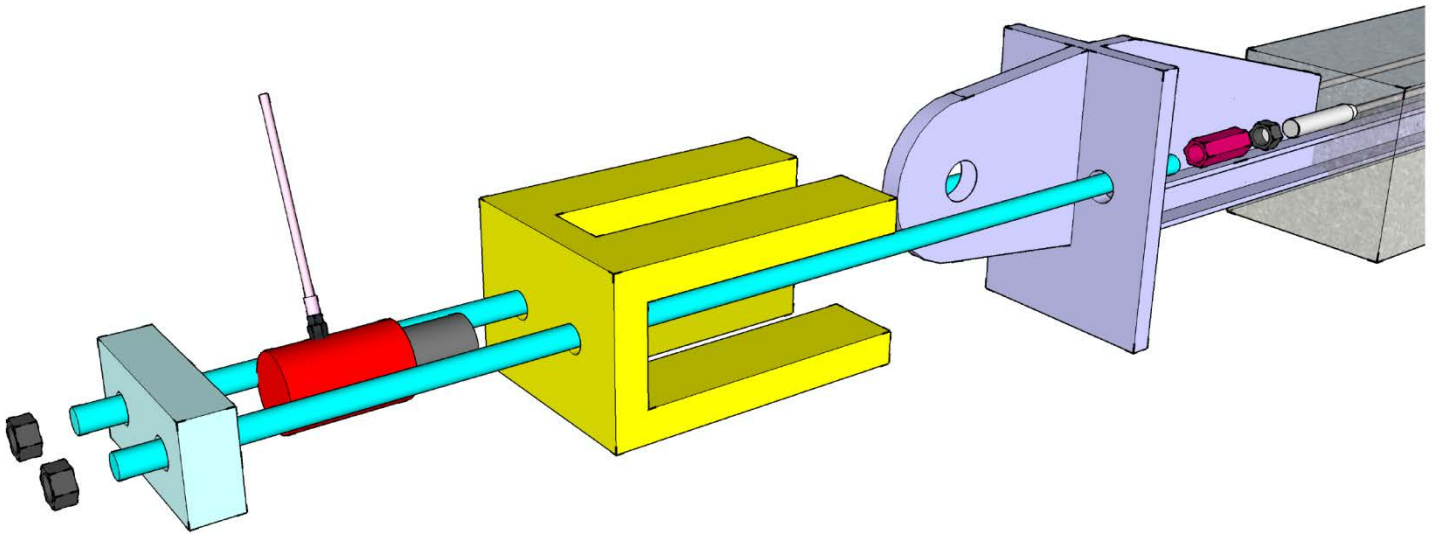


Fig. 1. PSRC members reinforced by prestressed tendons



(a) Exploded view of the post-tension hydraulic device



(b) Practicality picture of of the post-tension hydraulic device

Fig. 3. The post-tension hydraulic device

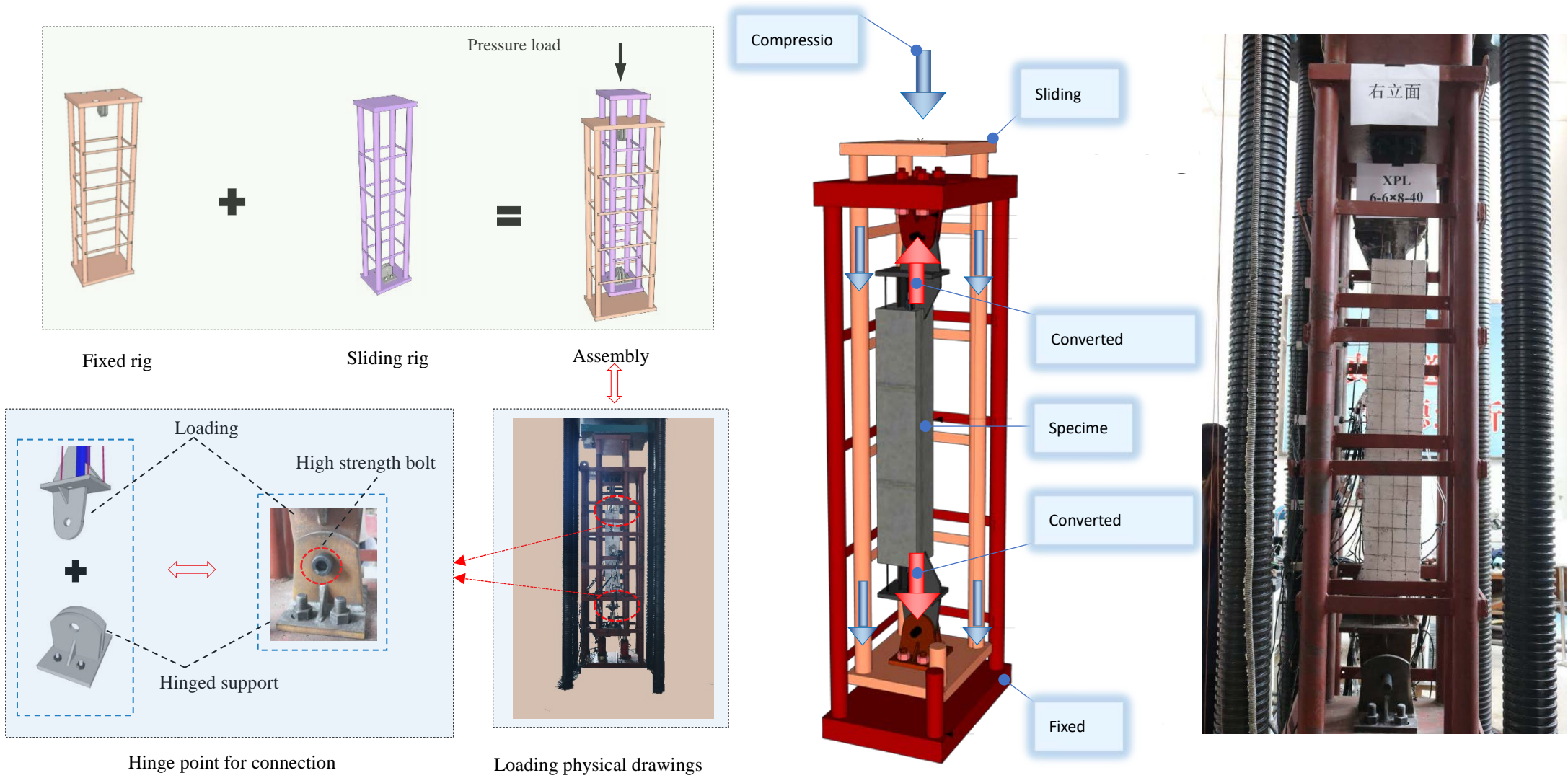


Fig. 4. Details of design and setup of the test rig

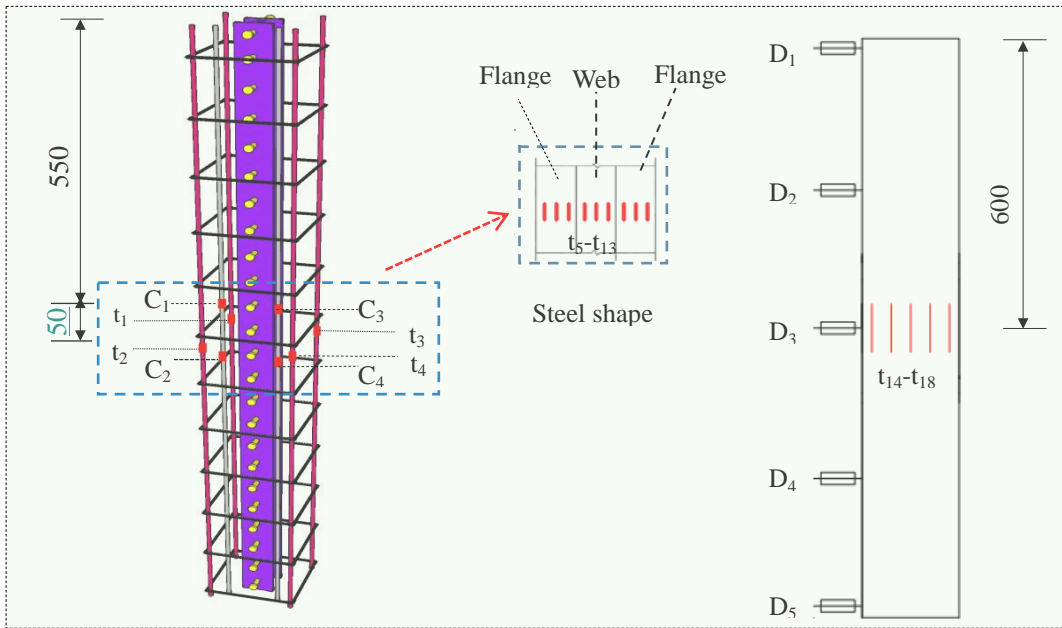
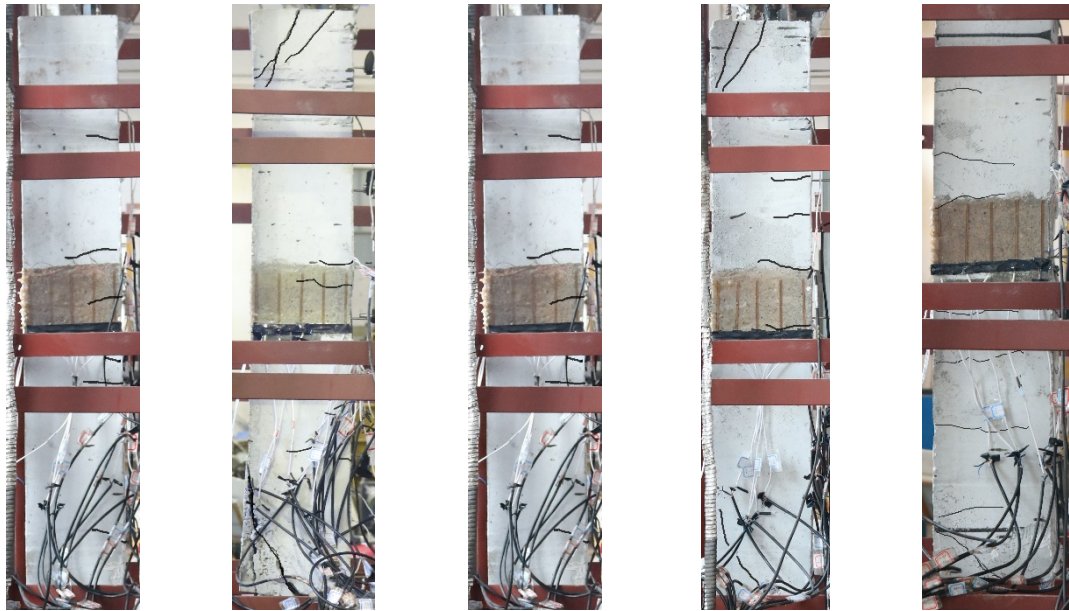


Fig. 5. Layout of measuring points across the specimens (Unit: mm)

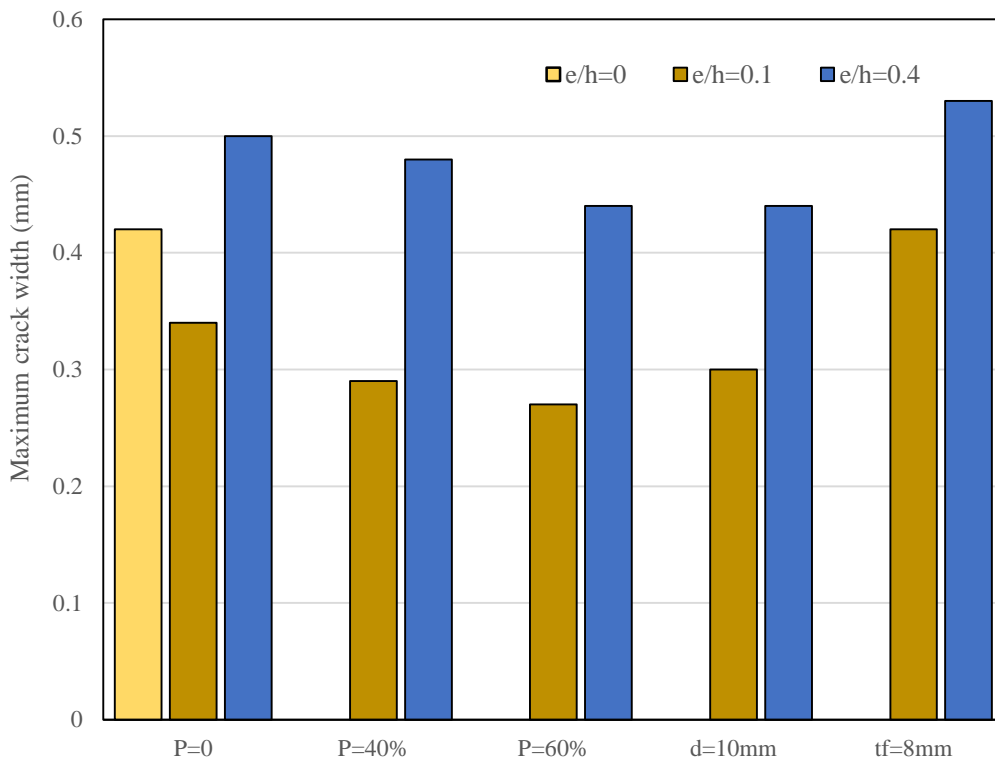


(a) APZ-6-6 (b) SPZ-6-6 (c) SPZ-6-6-40 (d) SPZ-6-6-60 (e) SPZ-10-6-40 (f) SPZ-6-8-40

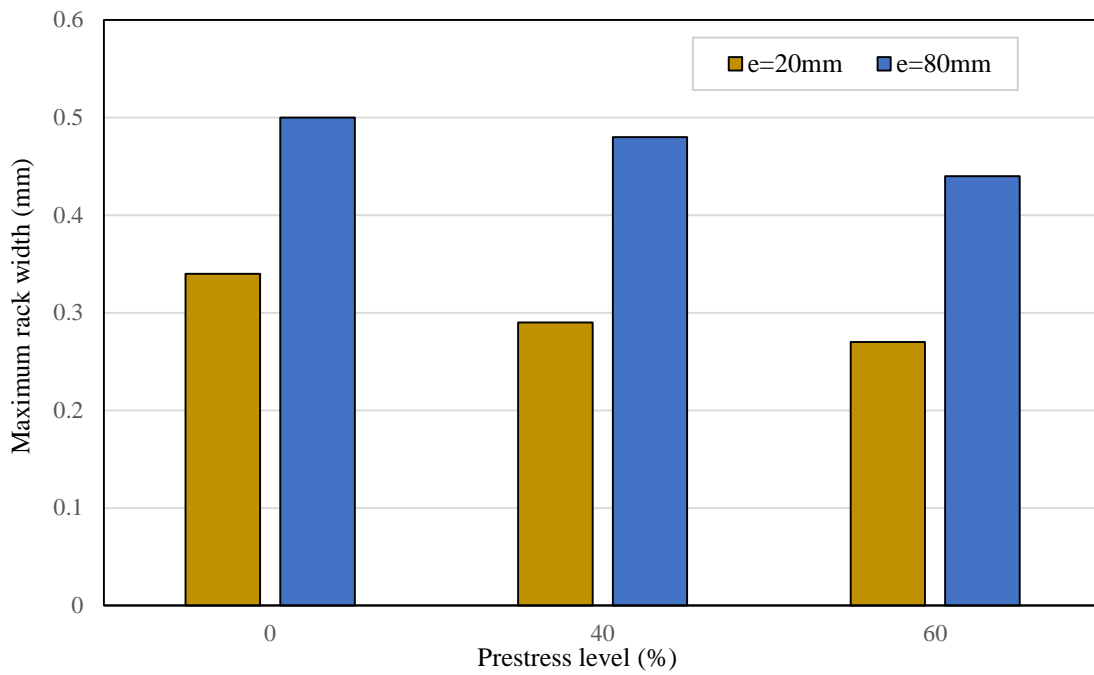


(g) LPZ-6-6 (h) LPZ-6-6-40 (i) LPZ-6-6-60 (j) LPZ-10-6-40 (k) LPZ-6-8-40

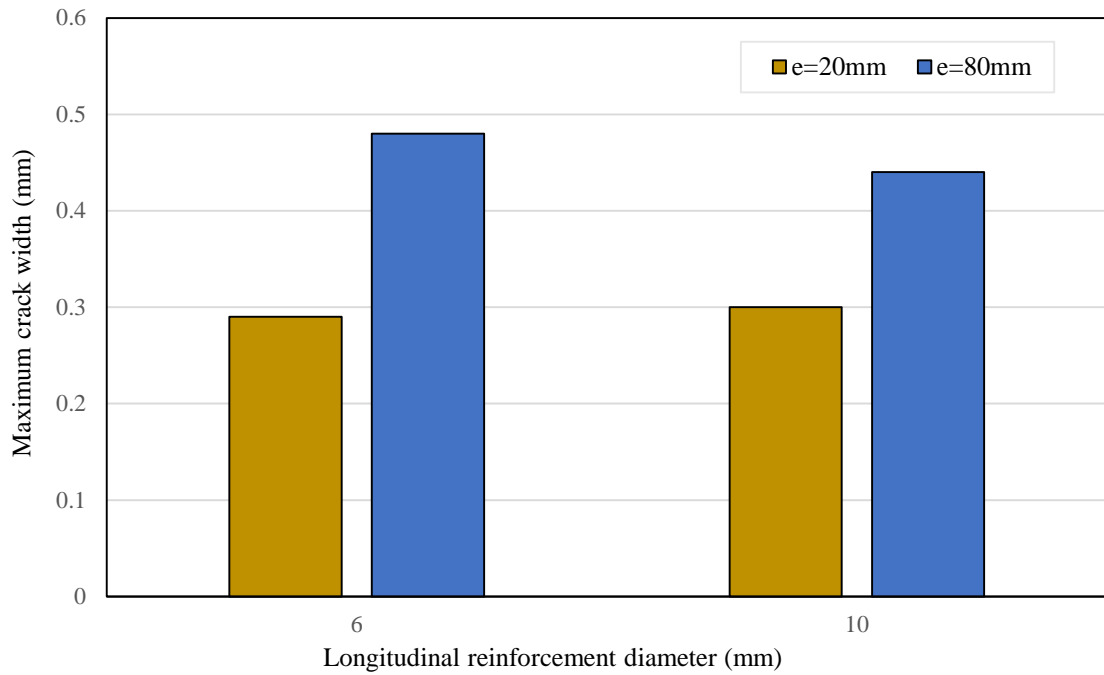
Fig. 6. Crack distribution of the ultimate shape of the specimen



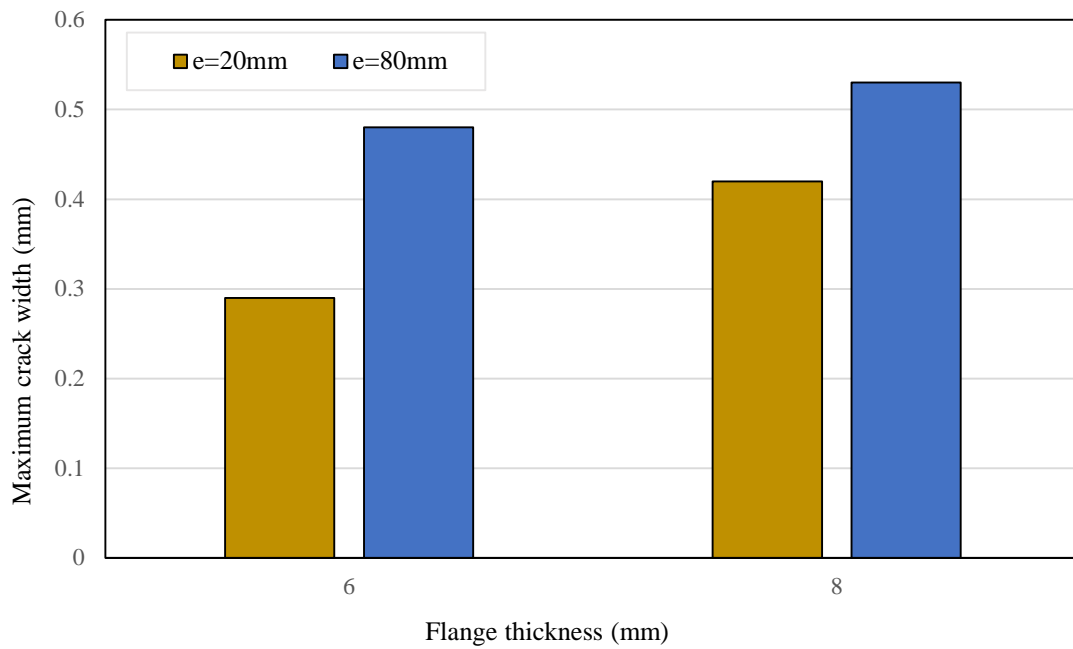
(a) Impact of eccentricity on maximum crack width



(b) Impact of prestress level on maximum crack width



(c) Impact of longitudinal reinforcement diameter on maximum crack width



(d) Impact of flange thickness on maximum crack width

Fig. 7. Parameter analysis of maximum crack width

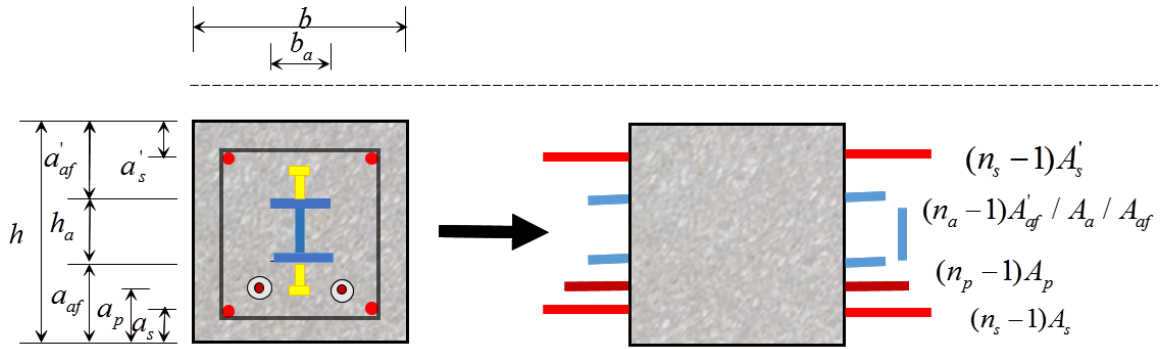


Fig. 8. Conversion section of steel reinforced concrete members with prestressed CFRP tendons

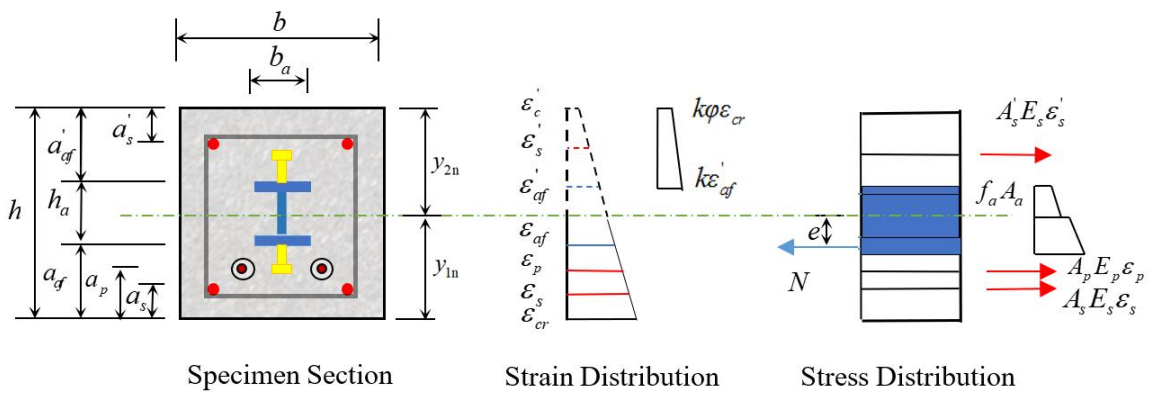


Fig.9. Strain distribution and internal forces across the depth of rectangle section

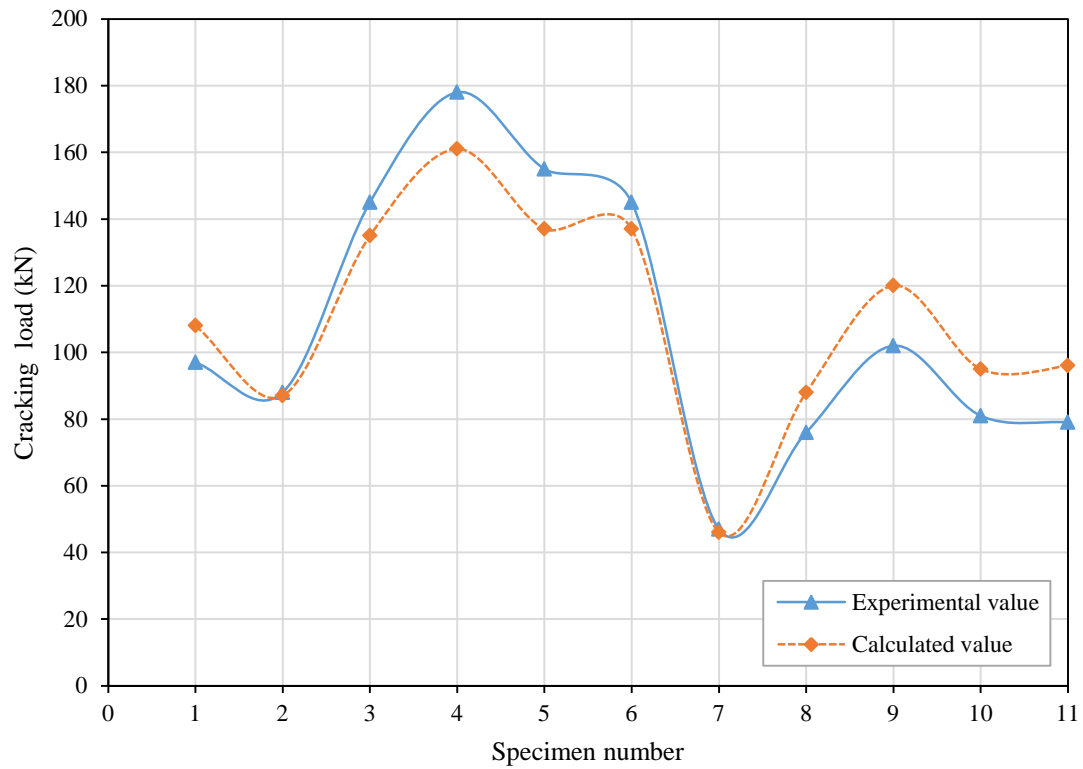


Fig. 10. Comparisons of cracking loading from the experiment and calculated results

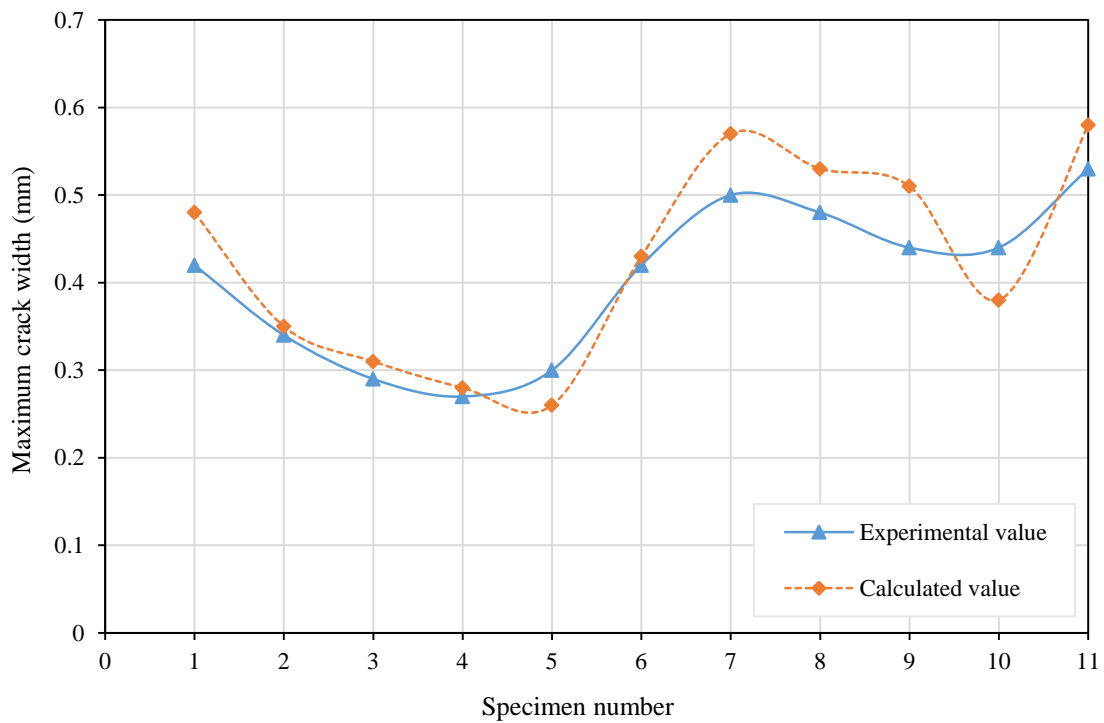


Fig. 11. Comparisons of maximum crack widths from the experiment and calculated results

Table 1

The design parameters of the specimens

Specimen	Eccentricity e (mm)	Eccentricity ratio e/h	Prestressed tension level λ (%)	Longitudinal reinforcement ρ	Flange thickness t_f (mm)
APZ-6-6	0	0	0	4C6	6
SPZ-6-6	20	0.1	0	4C6	6
SPZ-6-6-40	20	0.1	40	4C6	6
SPZ-6-6-60	20	0.1	60	4C6	6
SPZ-10-6-40	20	0.1	40	4C10	6
SPZ-6-8-40	20	0.1	40	4C6	8
LPZ-6-6	80	0.4	0	4C6	6
LPZ-6-6-40	80	0.4	40	4C6	6
LPZ-6-6-60	80	0.4	60	4C6	6
LPZ-10-6-40	80	0.4	40	4C10	6
LPZ-6-8-40	80	0.4	40	4C6	8

Table 2

Control load of CFRP tendons by tension

Tension level	0.2	0.4	0.6	0.8	1.0	1.05
$0.4 f_{ptk}^a$	5.9	11.8	17.6	23.5	29.4	30.9
$0.6 f_{ptk}$	8.8	17.6	26.5	35.3	44.1	46.3

^a f_{ptk} is the standard value of tensile strength of CFRP tendons.

Table 3

Mechanical property index of materials

Category	Name	Modulus of elasticity E (MPa)	Yield strength f_y (MPa)	Ultimate strength f_u (MPa)	Elongation of material δ (%)
Prestressed tendon	CFRP	1.54×10^5	1624	1910	—
Longitudinal reinforcement	C6	2.00×10^5	495	608	27.5
	C10	2.00×10^5	484	699	25.1
Steel shape	Q235	2.05×10^5	347	481	28.5
Loading plate	Q345	2.05×10^5	458	599	26.3

Table 4

Main test data

Specimen	Total prestress loss	Partial prestress loss	Maximum crack width	Cracking load	Variation of N_{cr} (%)	
	σ_i (N/mm ²)	σ_{i5}^a (N/mm ²)	ω_{max} (mm)	N_{cr} (kN)	λ_1^b	λ_2^c
APZ-6-6	—	—	0.42	97	—	0
SPZ-6-6	—	—	0.34	88	0	-9.3
SPZ-6-6-40	178.2	46.5	0.29	145	64.8	49.5
SPZ-6-6-60	218.5	69.8	0.27	178	102	83.5
SPZ-10-6-40	164.1	30.8	0.30	155	76.1	59.8
SPZ-6-8-40	175.3	49.3	0.42	145	84.8	49.5
LPZ-6-6	—	—	0.50	47	0	-51.5
LPZ-6-6-40	184	62.4	0.48	76	61.7	-21.6
LPZ-6-6-60	191	64.5	0.44	102	117	5.2
LPZ-10-6-40	166.6	59.9	0.44	81	72.3	-16.5
LPZ-6-8-40	163.2	47.9	0.53	79	68.1	-18.6

^a σ_{i5} is the prestressed loss caused by prestressed relaxation, concrete shrinkage and creep.

^b λ_1 is the rate of cracking load variation of prestressed members compared with ordinary eccentric members.

^c λ_2 is the change rate of cracking load of prestressed and ordinary members compared with axial tension members.

Table 5

Cracking load experimental values and calculation values of the specimens

Specimen	Experimental value $N_{cr,e}$ (kN)	Calculation value $N_{cr,c}$ (kN)	Ratio $N_{cr,e} / N_{cr,c}$	Calculation error μ_1^a (%)
APZ-6-6	97	107.5	0.90	10
SPZ-6-6	88	87	1.01	1
SPZ-6-6-40	145	135	1.07	7
SPZ -6-6-60	178	161.3	1.10	10
SPZ -10-6-40	155	137.8	1.12	12
SPZ -6-8-40	145	137.9	1.05	5
LPZ -6-6	47	46.9	1.02	2
LPZ -6-6-40	76	88.2	0.86	14
LPZ -6-6-60	102	120.8	0.84	16
LPZ -10-6-40	81.4	94.8	0.86	14
LPZ -6-8-40	79	95.5	0.83	17

$$^a \mu_1 = \left| 1 - N_{cr,e} / N_{cr,c} \right|$$

Table 6

Experimental and analytical values for maximum crack width of the specimens

Specimen	Experimental value	Calculation value	Ratio	Error
	$w_{\max,e}$ (mm)	$w_{\max,c}$ (mm)	$w_{\max,e} / w_{\max,c}$	μ_2^a (%)
APZ-6-6	0.42	0.48	0.88	12
SPZ-6-6	0.34	0.35	0.97	3
SPZ-6-6-40	0.29	0.31	0.94	6
SPZ -6-6-60	0.27	0.28	0.96	4
SPZ -10-6-40	0.30	0.26	1.15	15
SPZ -6-8-40	0.42	0.43	0.98	2
LPZ -6-6	0.50	0.57	0.88	12
LPZ -6-6-40	0.48	0.53	0.91	9
LPZ -6-6-60	0.44	0.51	0.86	14
LPZ -10-6-40	0.44	0.38	1.16	16
LPZ -6-8-40	0.53	0.58	0.91	9

$$^a \mu_2 = \left| 1 - w_{\max,e} / w_{\max,c} \right|$$